Dislocation Dynamics in Al-Li Alloys. Mean Jump Distance and Activation Length of Moving Dislocations

Hosson, J.Th.M. De; Huis in 't Veld, A.; Tamler, H.; Kanert, O.

Published in:
Acta Metallurgica

DOI:
10.1016/0001-6160(84)90127-5

Acta metall. Vol. 32, No. 8, pp. 1205–1215, 1984
Printed in Great Britain.

0001-6160/84 $3.00 + 0.00

DISLOCATION DYNAMICS IN Al–Li ALLOYS. MEAN JUMP DISTANCE AND ACTIVATION LENGTH OF MOVING DISLOCATIONS

J. Th M. De HOSSON, A. HUIS in't VELD

Department of Applied Physics, Materials Science Centre, University of Groningen, Nijenborgh 18, 9747 AG Groningen, The Netherlands

and

H. TAMLER, O. KANERT

Institute of Physics, University of Dortmund, 46 Dortmund 50, F.R.G.

(*Received* 19 *January* 1984)

Abstract—Pulsed nuclear magnetic resonance proved to be a complementary new technique for the study of moving dislocations in Al–Li alloys. The NMR technique, in combination with transmission electron microscopy and strain-rate change experiments have been applied to study dislocation motion in Al–2.2 wt% Li alloys, aged at 215°C (1 h) and 245°C (115 h). These heat treatments were chosen in order to obtain considerable differences in particle sizes which influence the mechanical properties. From the motion-induced part of the spin lattice relaxation rate, $T_{1\rho}^{-1}$ of ^{27}Al the mean jump distance of mobile dislocations has been measured as a function of strain. Transmission electron microscopic observations of the mean planar diameter of δ' precipitates, together with the NMR data, predicted the increase in yield stress of these alloys compared to ultrapure Al in agreement with experiments. In alloys aged 1 h at 215°C the precipitates are believed to be shearable. After aging 115 h at 245°C NMR and TEM observations indicated that the particles were not sheared. It was found that the activation length, obtained from mechanical strain-rate change experiments have different values compared to the values of the mean jump distance determined by NMR. Reasons for the mean jump distance being different from the activation length have been given. Nevertheless, there exists an internal consistency, namely: both mean jump distance and activation length have been found to decrease with strain hardening more rapidly in Al–Li containing nonshearable precipitates than in Al–Li containing shearable precipitates.

Résumé—La résonance magnétique nucléaire pulsée est une nouvelle technique complémentaire pour l'étude des dislocations en déplacement dans des alliages Al–Li. Nous avons utilisé la RMN, ainsi que la microscopie électronique en transmission et des expériences de changement de la vitesse de déformation pour étudier le déplacement des dislocations dans des alliages Al–2,2% Li (en poids) vieillis à 215°C (1 h) et à 245°C (115 h). Nous avons choisi ces traitements thermiques afin d'obtenir des différences considérables dans les tailles de particules, qui influencent les propriétés mécaniques. Nous avons mesuré la distance de saut moyenne pour les dislocations mobiles en fonction de la déformation à partir de la partie de la vitesse de relaxation spin-réseau de ^{27}Al induite par le mouvement $T_{1\rho}^{-1}$. Des observations du diamètre planaire moyen des précipités δ' par microscopie électronique en transmission, associées aux résultats de la RMN, ont permis de prévoir l'accroissement de la limite élastique de ces alliages par rapport à l'aluminium ultrapur, en accord avec les expériences. Dans les alliages vieillis 1 h à 215°C, nous pensons que les précipités peuvent être cisaillés. Après vieillissement de 115 h à 245°C, la RMN et la MET ont montré que les particules n'étaient pas cisaillées les valeurs de la longueur d'activation, obtenues à partir des expériences de changement de la vitesse de déformation mécanique, étaient différentes des valeurs de la distance de saut moyenne déterminées par RMN. Nous proposons des explications pour cette différence entre les valeurs de la distance de saut moyenne et la longueur d'activation. Néanmoins, il existe une cohérence interne: la distance de saut moyenne et la longueur d'activation diminuent avec le durcissement plus rapidement dans Al–Li contenant des précipités non cisaillables que dans Al–Li contenant des précipités cisaillables.

Zusammenfassung—Gepulste Kernspinresonanz hat sich als eine neue ergänzende Meßmethode zur Untersuchung der Versetzungsbewegung in Al–Li erwiesen. Sie wurde zusammen mit des Durchstrahlungselektronenmikroskopie und mit Geschwindigkeitswechseln auf die Versetzungsbewegung in Al–2,2 Gew.-% Li, die bei 215°C für 1 h oder bei 245°C für 115 h ausgelagert worden waren, angewendet. Mit diesen Wärmebehandlungen wurden beträchtliche Unterschiede in den das mechanische Verhalten beeinflussende Teilchengrößen erhalten. Aus dem bewegungsinduzierten Teil der Spingitterrelaxationsrate $T_{1\rho}^{-1}$ des ^{27}Al wurde die mittlere Sprungweite der beweglichen Versetzungen in Abhängigkeit von der Dehnung gemessen. Durchstrahlungselektronenmikroskopische Beobachtungen der mittleren ebenen Durchmesser der δ'-Ausscheidungen ergaben zusammen mit den Kernspinresonanzmessungen eine erhöhte Fließspannung dieser Legierungen im Vergleich zu ultrareinem Al, in übereinstimmung mit den Experimenten. In den Legierungen mit einstündiger Auslagerung bei 215°C sind die Ausscheidungen wohl scherbar. Elektronenmikroskopie und Kernspinresonanz zeigen, daß sie nach Auslagerung bei 245°C für 115 h nicht geschert werden. Die Aktivierungslängen, die aus den mechanischen Geschwindigkeitswechselversuchen erhalten wurden, unterscheiden sich von den Sprunglängen aus der Kernspinresonanz. Gründe für diesen Unterschied werden angeführt. Nichtsdestoweniger gibt es eine innere Verträglichkeit: sowohl mittlere Sprungweite als auch Aktivierungslänge nehmen mit der Verfestigung rascher in Al–Li-Legierungen mit nicht-scherbaren Ausscheidungen ab als in Legierungen mit scherbaren Ausscheidungen.

1. INTRODUCTION

Aluminium–lithium based alloys offer considerable promise for structural applications, especially in aerospace industry [1], since they possess the potential for high strength in combination with a lower density and a higher modulus of elasticity than conventional aluminium alloys. The strengthening mechanism of Al–Li alloys is due to the formation of coherent δ' precipitates [2] (ordered $L1_2$ phase Al_3Li). To understand the strengthening mechanism we have investigated the way in which moving dislocations interact with precipitate particles of the coherent phase δ'. In this paper, a nuclear magnetic resonance study of the mechanism of dislocation motion in Al–2.2 wt% Li is reported. The *in situ* nuclear spin relaxation measurements provide information about the effective mean jump distance of mobile dislocations. In addition, the activation length of mobile dislocations has been obtained from strain-rate change experiments on Al-2.2 wt% Li. Both the mean jump distance and the activation length were related to the *static* transmission electron microscopic observations of the instantaneous configuration of dislocations and the precipitates. The experiments were carried out on Al–Li alloys aged at two different temperatures: 215°C (1 h) and 245°C (115 h). These heat treatments were chosen in order to obtain considerable differences in particle sizes which influence the mechanical properties and dislocation dynamics.

2. THEORETICAL BACKGROUND

A few years ago, we showed that pulsed nuclear magnetic resonance is a useful tool to study dislocation motion. It turned out that three sets of microscopic information about the dislocation motion can be deduced in principle from these experiments:

(i) the mean jump distance of moving dislocations,
(ii) the mean time of stay between two consecutive jumps of a mobile dislocation; and
(iii) the mobile dislocation density as a fraction of the total dislocation density.

While *static* quadrupolar effects associated with static lattice defects such as dislocations are analyzed in terms of width, line shape and intensity of the NMR signal, *dynamical* effects, such as dislocation motion during plastic deformation, are studied through the related nuclear spin-lattice relaxation process. Nevertheless, both experimental methods are essentially based on the interaction between nuclear electric quadrupole moments and electric field gradients at the nucleus. Around a dislocation in a cubic crystal the symmetry is destroyed and interactions between nuclear electric quadrupole moments and electric field gradients arise. Whenever a dislocation changes its position in the crystal, the surrounding atoms have also to move, thus causing time fluctuations both of the quadrupolar and dipolar spin Hamiltonian for spins with $I > \frac{1}{2}$. However, dipolar effects on the nuclear spin relaxation due to dislocation motion are negligible and quadrupolar interactions dominate the observed relaxation behaviour. Furthermore, for the investigation of rather infrequent defect motions as in the case of moving dislocations, the spin-lattice relaxation time in the rotating frame, $T_{1\rho}$, has proved to be the most appropriate NMR parameter affected by such motions. For detailed information of this technique reference is made to previous work [3–6]. Only a concise review will be given here.

While deforming a sample with a constant strain rate $\dot{\epsilon}$ the spin-lattice relaxation rate in a (weak rotating) applied field H_1, $(1/T_{1\rho})$ of the resonant nuclei in the sample is enhanced due to the motion of dislocations. The resulting expression for the relaxation rate induced by dislocation motion is given by

$$\left(\frac{1}{T_{1\rho}}\right)_D = \frac{A_Q}{H_1^2 + H_{L\rho}^2} \frac{\rho_m}{\tau_w} \tag{1}$$

where A_Q depends on the mean-squared electric field gradient due to the stress field of a dislocation of unit length and the quadrupolar coupling constant. $H_{L\rho}$ is the mean local field in the rotating frame determined by the local dipolar field $H_{D\rho}$ and the local quadrupolar field $H_{Q\rho}$. ρ_m and τ_w represent the mobile dislocation density and the waiting time of a mobile dislocation, respectively. The deformation experiments are carried out in a magnetic field of 1.4 T with a constant deformation rate $\dot{\epsilon}$. This type of experiment is governed by Orowan's equation [7]. Assuming a thermally activated jerky motion of mobile dislocations, the macroscopic strain rate is given by (steady state mobile density) [8]

$$\dot{\epsilon} = \phi b \rho_m L / \tau_m \tag{2}$$

where τ_m is the mean time of stay between successive jumps (waiting time τ_w plus actual jump time τ_j). b is the magnitude of the Burgers vector, ϕ is a geometrical factor, and L is the mean jump distance. Since $\tau_m \simeq \tau_w (\tau_j \ll \tau_w)$ follows for the spin lattice relaxation rate [equation (1)] using equation (2):

$$\left(\frac{1}{T_{1\rho}}\right)_D = \frac{A_Q}{H_1^2 + H_{L\rho}^2} \frac{1}{\phi b L} \dot{\epsilon}. \tag{3}$$

Hence, for a given plastic deformation rate $\dot{\epsilon}$ the nuclear spin relaxation rate is proportional to the inverse of the mean jump distance L. A_Q and $H_{L\rho}^2$ have been obtained separately from a line shape analysis of the NMR signal [9] and spin echo NMR measurements [10]. Relationship (3) has been used to determine L as a function of strain.

On the other hand, the strain rate can be written as [8]

$$\dot{\epsilon} = \dot{\epsilon}_0 \exp\left(-\frac{\Delta G}{kT}\right) \tag{4}$$

where ΔG is the activation energy for intersection, assuming that the only release of a dislocation segment from an obstacle is due to thermal fluctuations. The Arrhenius' type of behaviour of $\dot{\epsilon}$ holds for the asymptotic flow stress [11]. The apparent activation volume is defined as

$$V = -\left(\frac{\delta \Delta G}{\delta \tau}\right)_T = kT\left(\frac{\delta \ln \dot{\epsilon}}{\delta \tau}\right)_T \simeq \lambda b^2 \qquad (5)$$

where $\dot{\epsilon}_0$ is taken to be independent of the shear stress $\tau \cdot \lambda$ represents the average obstacle spacing or the activated minimum length. Mechanical tests involving a change in strain rate by a factor of ten have been employed to measure $(\delta \ln \dot{\epsilon}/\delta\tau)_T$, equation (5), from which the apparent activation volume and average spacing λ have been deduced.

3. EXPERIMENTAL

Polycrystalline samples with a grain size of the order of 100–200 μm were used. To avoid skin effect distortion of the NMR signal the NMR experiments were carried out on rectangular foils of size 27 mm $\times$ 12 mm $\times$ 40 μm. The starting material for the Al–Li samples was Al–2.5 wt% Li. After a homogenizing procedure at 580°C for 1 h the material was rolled out to the aforementioned thickness and has then been cut by spark erosion to the sample size given above. Afterwards, the samples were annealed a second time at 580°C for 7 min and quenched in water. In order to produce δ' precipitates of different sizes the samples were exposed to a third heat treatment (either 1 h at 215°C or 115 h at 245°C). After the heat treatments, the Li content was measured by means of a Perkin–Elmer spectrophotometer and appeared to be equal to 2.2 wt%

In the NMR experiment, the sample under investigation is plastically deformed by a servo-hydraulic tensile machine (ZONIC Technical Lab. Inc., Cincinnati) of which the exciter head XCI 1105 moves a driving rod with a constant velocity. While the specimen was deforming, ^{27}Al nuclear spin measurements were carried out by means of a BRUKER pulse spectrometer SXP 4-100 operating at 15.7 MHz corresponding to a magnetic field of 1.4 T controlled by an NMR stabilizer (BRUKER B-SN 15). The NMR head of the spectrometer and the frame in which the rod moves formed a unit which was inserted between the pole pieces of the electromagnet of the spectrometer. The set-up of the whole tensile testing system is described in [5]. A scheme of the experimental set-up is displayed in Fig. 1. As shown in this block diagram, the spectrometer was triggered by the electronic control of the tensile machine. The trigger starts the nuclear spin relaxation experiment at a definite time during the deformation determined by the delay time of the trigger pulse. Immediately before and after the plastic deformation the mag-

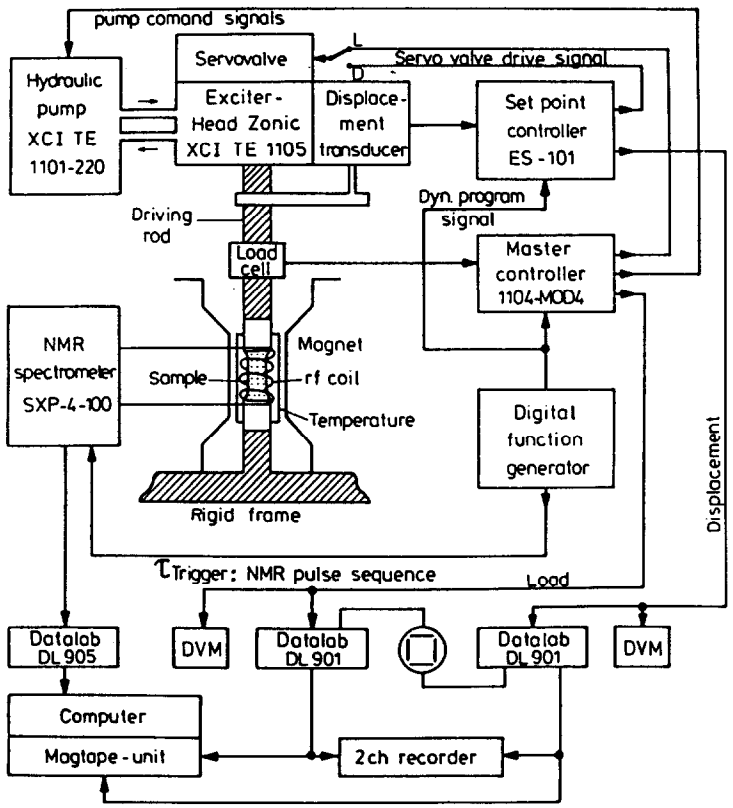

Fig. 1. Block scheme of the experimental set-up, consisting of the deformation equipment, NMR spectrometer and magnet, data recording and handling instruments.

nitude of the background (conduction-electron) relaxation time $(T_{1\rho})_0$ was measured. From the experimental $T_{1\rho}$-data, the dislocation induced contribution of the relaxation time, $(T_{1\rho})_D$, could be determined, according to

$$\frac{1}{T_{1\rho}} = \left(\frac{1}{T_{1\rho}}\right)_0 + \left(\frac{1}{T_{1\rho}}\right)_D. \tag{6}$$

To be sure that the increase in the nuclear spin relaxation rate during plastic deformation with $\dot{\epsilon} = \text{constant}$ is caused actually by internal atomic motions and not by any kind of external electrodynamic effects, $(T_{1\rho})^{-1}$ was measured while moving the whole sample with a constant velocity but without deformation. No change within experimental error in the relaxation rate was observed in such an experiment.

The NMR and mechanical measurements discussed here were carried out at 77 K. At such a low temperature nuclear spin relaxation effects due to diffusive atomic motions are negligible. Taking the Einstein–Smoluchowski equation as a starting point for connecting the diffusion coefficient with the mean time of stay τ_c of an atom between two diffusion jumps (neglecting correlation effects) the correlation times for atomic jumps of ^{27}Al and Li in the aluminium matrix can be calculated at 77 K. These calculations indicate that ^{27}Al and Li are actually immobile. The correlation times ($> 10^{70}$ s) are much larger than typical values of τ_w for mobile dislocations ($\simeq 10^{-4}$ s with $\dot{\epsilon} \simeq 1\,\text{s}^{-1}$). Consequently, an observable contribution of diffusive atomic motions to $T_{1\rho}$ does not occur.

Transmission electron micrographs were taken by using a JEM 200 CX operating between 120 and 160 kV. Disc-type specimens were obtained from the deformed foils by spark cutting to minimize deformation. The samples were electrochemically thinned in polishing equipment at room temperature in a solution of 49% methanol, 49% nitric acid, 2% hydrochloric acid. Dislocations were imaged in dark-field using the weak-beam technique [12].

4. RESULTS AND DISCUSSION

4.1. Mean jump distance

In Fig. 2 the mean jump distance measured by NMR in Al–Li aged at 215°C (1 h) is illustrated as a function of strain. The spin lattice relaxation rate was determined at a constant strain rate $\dot{\epsilon} = 1.6\,\text{s}^{-1}$. The shape of the L vs ϵ curve is quite similar to the curve obtained for ultrapure Al using NMR techniques [4]. Apparently at the beginning of deformation the storage of dislocations follows strictly geometrical or statistical rules. Assuming that the mean jump distance is proportional to the slip line length Λ_L which decreases with increasing strain in pure f.c.c. metals, it means that

$$\frac{1}{L} \approx \epsilon. \tag{7}$$

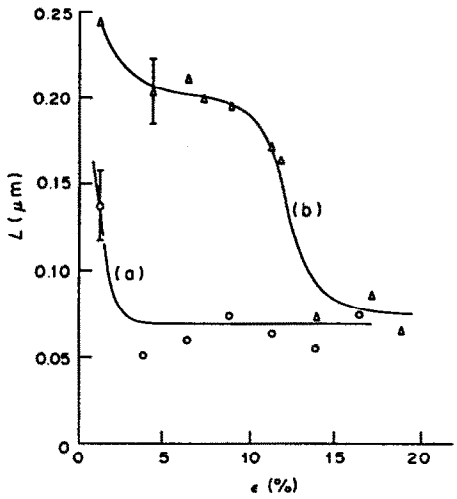

Fig. 2. The mean jump distance measured by NMR as a function of strain ϵ in (a) Al–2.2 wt% Li aged at 215°C (1 h) and (b) Al–2.2 wt% Li aged at 245°C (115 h). Each data point represents the averaged value over 5 measurements. The error bar indicates the deviation within a set of L-data at a particular ϵ ($\dot{\epsilon} = 1.6\,\text{s}^{-1}$).

An electron micrograph illustrating the microstructure of deformed Al–Li till fracture is shown in Fig. 3. δ' superlattice reflections have been used for imaging the Al_3Li precipitates (dark field/strong beam, $\mathbf{g} = [001]$). The appearance of superlattice dislocations in this alloy shown in Fig. 4 (dark field/weak beam image) indicates that the precipitates are shearable. Stereo-electron micrographs revealed that the volume fraction f is about 3% and the mean diameter $2\bar{R}$ of the precipitates is about 15 nm leading to a Friedel spacing of 0.08 μm and a mean square spacing of 0.06 μm. The square lattice spacing of the particles is calculated from

$$L_s = \left(\frac{\pi}{f}\right)^{1/2} \bar{R}_s \tag{8}$$

and the Friedel spacing is defined as [13]

$$L_F = \left(\frac{\pi T \bar{R}_s}{\gamma f}\right)^{1/2} \tag{9}$$

where T represents the line tension ($\simeq 0.5\,\mu b^2$, $\mu = 0.3 \cdot 10^5$ MPa) and $\bar{R}_s$ is the mean planar radius of the particles ($\pi/4\,\bar{R}$). From the separation between the two ordinary unit dislocations constituting a superlattice dislocation (96 nm in Fig. 4) an antiphase boundary energy $\gamma = 140\,\text{mJ/m}^2$ has been found. Both values L_s and L_F are close to the mean jump distance L measured by NMR. However, the mean jump distance is much larger than the average particle diameter $\bar{d}$. Therefore, the δ' ordered precipitates are considered to be perfectly sheared off during deformation. If n dislocations of Burgers vector b shear a particle, then the cross section of the precipitate in the slip plane will be reduced by an amount nb. Consequently, the effective planar diameter of the particle can be considered to decrease as the strain increases. Since the flow stress is proportional to $(\bar{d})^{1/2}$ [14], the flow resistance on an identical slip plane decreases as

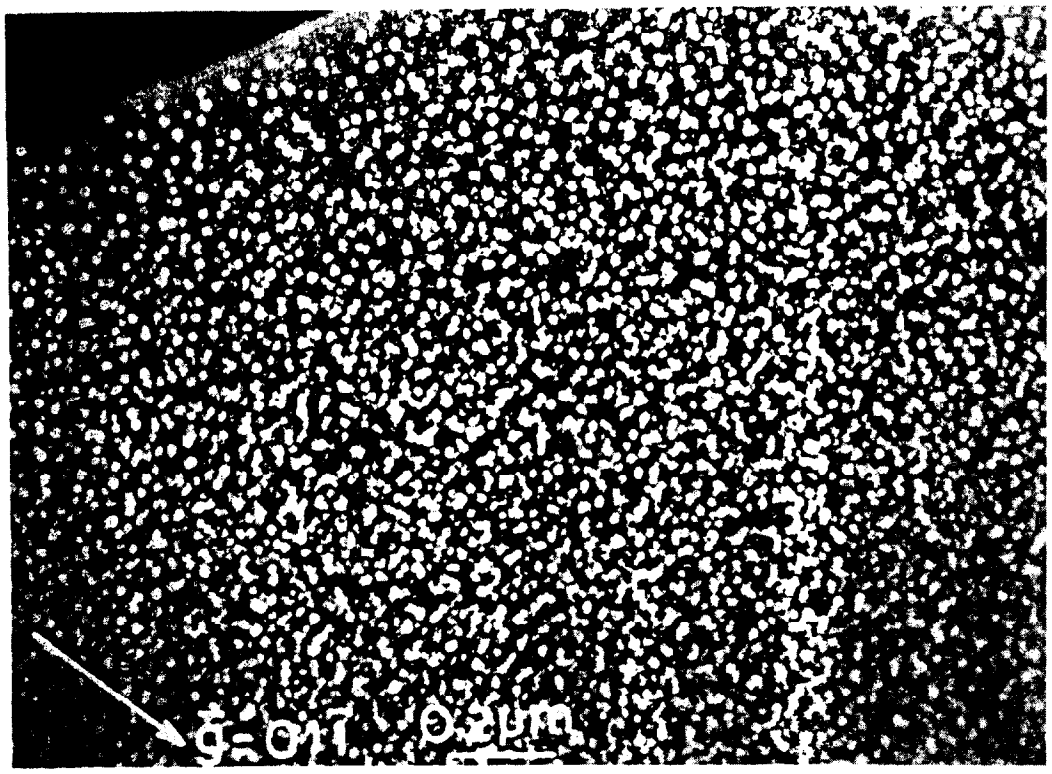

Fig. 3. Al–2.2 wt% Li aged at 215°C (1 h) deformed till fracture g = [01Ī].

the strain increases. The slip plane is thus work-softened so that further slip will tend to concentrate on that plane. After the passage of some pairs of superlattice dislocations (which were only imaged in the electron microscope when $\epsilon \leqslant 5\%$) the ordered precipitates are finally sheared off completely. Then, *single* dislocations become easily mobile, leading to the formation of the arrays of pile-up dislocations

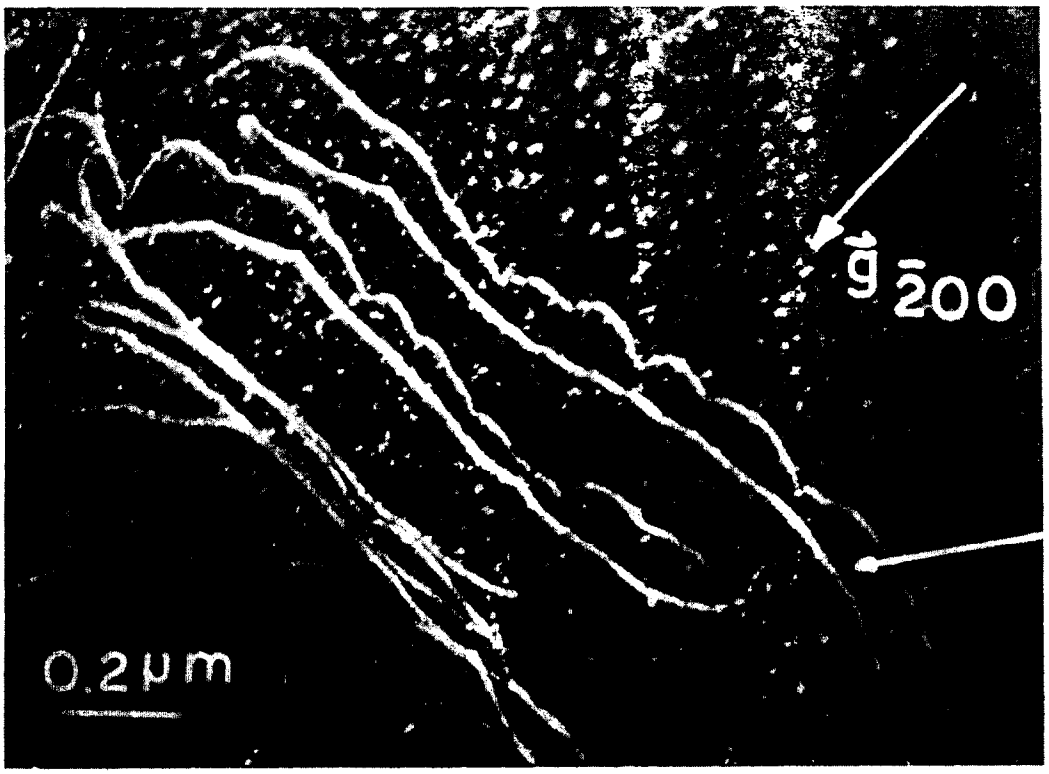

Fig. 4. Al–2.2 wt% Li aged at 215°C (1 h) deformed 5% at 77 K. Dark field weak beam image, [011] orientation, g = [2̄00]. Superlattice dislocation imaged: $\frac{1}{2}$[101](Ī11)

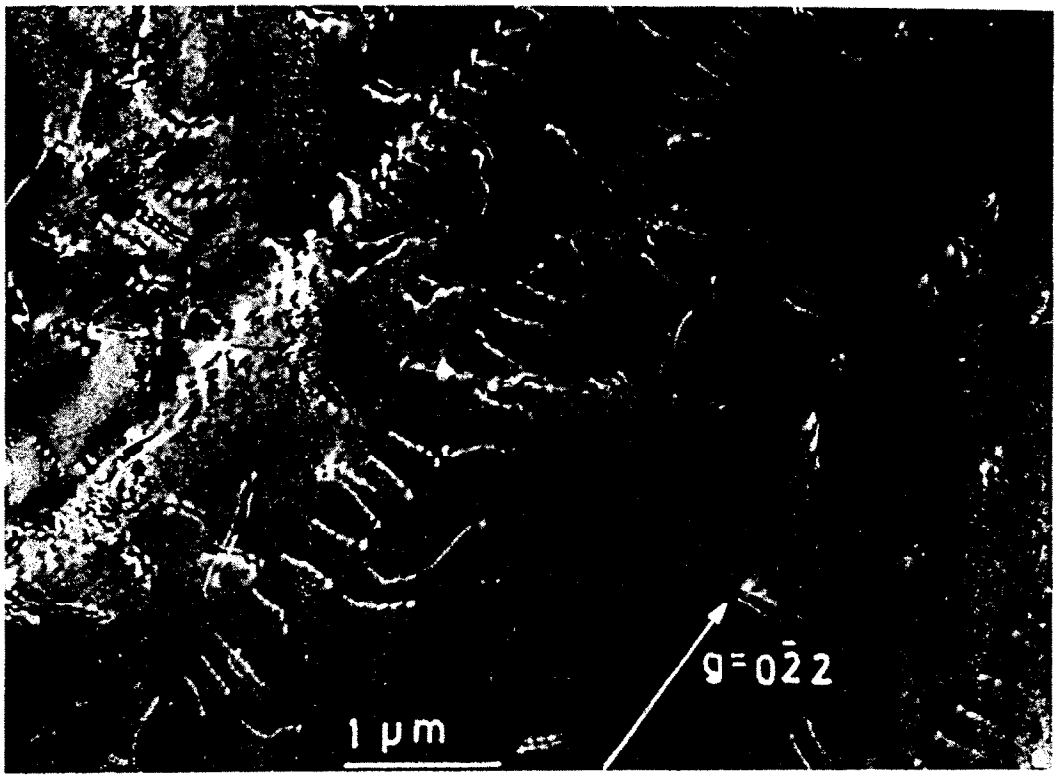

Fig. 5. A pile-up of coupled dislocations in Al–2.2 wt% Li aged at 215°C (1 h) deformed till fracture at 77 K. Dark field/weak beam image, $\mathbf{g} = [0\bar{2}2]$.

(see Fig. 5) [15]. Near the head of the pile-up, the dislocations are obviously paired but the pair spacing increases for dislocations further toward the tail until after a number of dislocations they become uncoupled.

At aging temperatures above 230°C coarsening of the precipitates occurred. In Fig. 6 a stereo micrograph of an Al–Li sample (undeformed) aged at 230°C for 17 h is shown. By using two diffraction spots, namely a superlattice reflection and a matrix reflection, dislocations as well as precipitates are imaged. A row of δ' precipitates are preferentially nucleated on a matrix dislocation. After aging at 230°C collinear rows of extra large precipitates were observed, sometimes elongated along the line direction. In those cases a dislocation was found to be associated with the rows, lying on the common line between particles and on the surface of the particles themselves. This may be explained by pipe diffusion.

The mean jump distance of moving dislocations in Al–2.2 wt% Li aged at 245°C (115 h) as a function of strain is displayed in Fig. 2.

Figure 7 shows an electron micrograph (dark field/weak beam, $\mathbf{g} = [02\bar{2}]$) of the Al–Li alloy de-

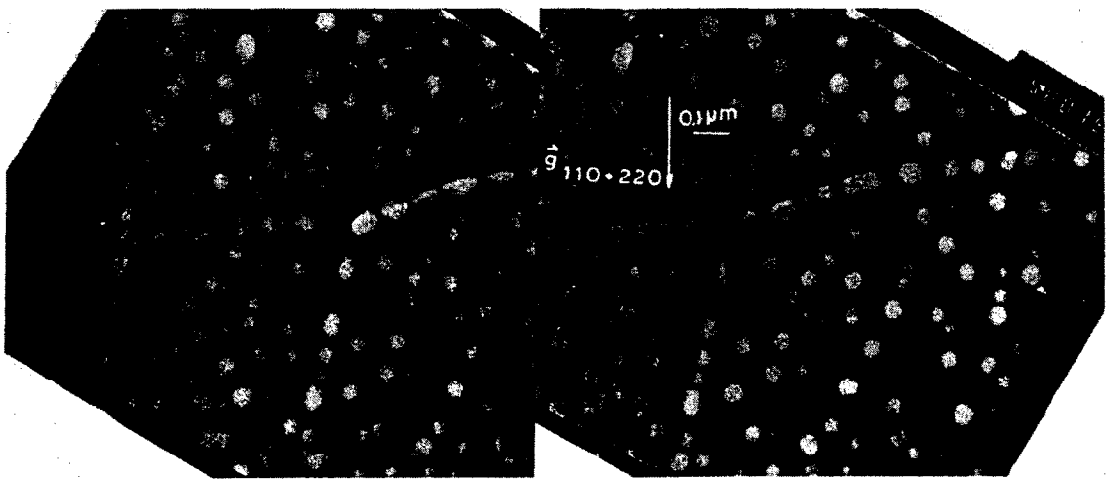

Fig. 6. Al–Li (2.2 wt%) aged at 230°C for 17 h, $\mathbf{g} = [110] + [220]$, stereo angle 24°.

Fig. 7. Al–Li (2.2 wt%) aged at 245°C for 115 h. Deformed till fracture. $\mathbf{g} = [00\bar{1}] + [02\bar{2}]$.

formed till fracture. In this case the microstructure as well as the NMR results look very different compared to those of Al–Li aged at 215°C (1 h). From stereo electron micrographs the average gap between the precipitates, L_p, is found to be 0.3 μm ($\bar{R} = 0.14\,\mu$m, $f = 5\%$). This value is close to the mean jump distance of 0.25 μm determined by NMR at low ϵ, indicating that in contrast to Al–Li aged at 215°C (1 h), Orowan hardening might be the predominant hardening mechanism. Figure 7 clearly shows that looping occurred during plastic deformation. The interparticle spacing in the slip direction sets an upper limit for the slip distance, i.e. the actual distance traversed before a dislocation gets stuck. The hardening is expected to be controlled by the microstructure at the beginning of deformation. At higher strain values the mean jump distance is decreasing gradually from 0.2 μm at $\epsilon = 5\%$ to 0.08 μm. The reason for this decrease is two-fold: first of all "statistically stored" dislocations, i.e. those that would accumulate during simple tension, will diminish the mean jump distance substantially. As can be deduced from Fig. 7 the mean distance between the statistically stored dislocations is certainly much smaller than the mean separation of the δ' precipitates. If moving dislocations are delayed at each intersection with the statistically stored dislocations during a period $\tau_c > 10^{-4}$ s, spin lattice relaxation takes place. As a result of the spin lattice relaxation $T_{1\rho}^{-1}$ is determined by waiting time at each intersection. The mean jump distance is therefore decreasing upon deformation from the mean particle spacing at the beginning of deformation to the spacing between statistically stored dislocations later on. Secondly, since it is unlikely that each precipitate is to be intersected by only one slip plane, loops are expected to form vertical stacks. Any movement of dislocation debris accumulated round these particles affect the spin lattice relaxation rate as well.

The experimental results obtained are in agreement with the stress strain equation given by Ashby's concept of "statistically stored" and "geometrically necessary" dislocations, i.e. those generated to accomplish the rotation of the non-deforming particles during deformation [16, 17], namely

$$\sigma \approx \mu b (\rho_G + \rho_u)^{1/2} \tag{10}$$

where the density ρ_G of geometrically necessary dislocations is given by

$$\rho_G \simeq \left(\frac{1}{\Lambda_G}\right)\frac{4\epsilon}{b}. \tag{11}$$

The geometric slip distance Λ_G is $\bar{R}\sqrt{f}$ (R is the planar particle radius and f the volume fraction). Λ_G is considered to be characteristic of the microstructure and independent of the strain. The upper limit Λ_G in Al–Li containing nonshearable precipitates is calculated to be $\simeq 1\,\mu$m. Thompson *et al.* [18] proposed a modification to equation (10) where Λ_G sets an upper limit to Λ_u, the slip distance for a statistical storage, and $\Lambda_u \simeq \Lambda_G$ at yield. Then at small strain the slip distance is Λ_G and at large strain where $\Lambda_u \ll \Lambda_G$ it reduces to $\tau \sim \Lambda_u^{-1}$. This situation has been found in our experiments.

Figure 2 indicates that there exists a clear difference in functional dependence of L upon ϵ in these two Al–Li alloys. The mean jump distance is almost constant for $\epsilon \gtrsim 5\%$ in Al–Li containing shearable precipitates whereas L is still a decreasing function of ϵ in Al–Li containing nonshearable precipitates. These differences in behaviour are in agreement with the various workhardening rates. According to equation (2) the shear strain can be described by the mean jump distance L of the mobile dislocations according to $a = b\rho_m L$. In general, the flow stress can be expected to vary with dislocation density according to: $\tau = \alpha\mu b\sqrt{\rho}$. This gives the workhardening rate θ as

$$\frac{\delta\tau}{\delta a} = \frac{\alpha\mu}{2\sqrt{\rho}\left[\rho_m\left(\frac{dL}{d\rho}\right) + L\left(\frac{d\rho_m}{d\rho}\right)\right]}. \tag{12}$$

If L is assumed to be constant, θ becomes proportional to $1/L$ and ρ_m must increase with ρ according to $\rho_m \approx \sqrt{\rho}$. This is the situation for Al–Li containing shearable precipitates when $\epsilon \gtrsim 5\%$.

In contrast, since L is not constant up to $\epsilon = 15\%$ in Al–Li containing nonshearable precipitates

$$\frac{dL}{d\rho} \neq 0. \tag{13}$$

If L is not a constant, equation (12) can be rewritten in terms of the internal stress τ_i as (A is a constant)

$$\theta = \frac{A}{\tau_i\frac{d\bar{L}}{d\tau_i} + L} \tag{14}$$

neglecting the thermal component of the flow stress which is much smaller than the athermal component in the case of f.c.c. metals. Since $(dL/d\rho)$ and $(dL/d\tau_i)$ are both negative ($L \approx \rho^{-1/2}$), the workhardening rate of Al–Li containing nonshearable precipitates is expected to be higher than θ of Al–Li containing shearable precipitates. Indeed, this is confirmed by the experimental σ–ϵ curves depicted in Fig. 8.

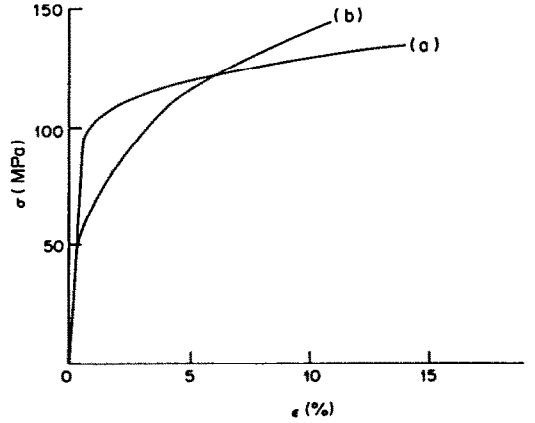

Fig. 8. Experimental stress–strain curve of *some* of the foils measured at 77 K. (a) Al–Li (2.2 wt%) aged at 215°C (1 h), (b) Al–Li (2.2 wt%) aged at 245°C (115 h).

The values of the mean jump distance obtained by NMR can be used for a theoretical evaluation of the yield stress. The yield stress of ultrapure Al at 77 K appeared to be equal to 10 MPa. Consequently, the increase of the yield stress of the samples aged at 215°C and aged at 245°C, compared to ultrapure Al, is 92 and 41 MPa, respectively (see Fig. 8). A calculation of the flow stress for a single dislocation, τ_1, taking into account the effective obstacle spacing as a function of applied stress for finite obstacles and slightly bent dislocations, has been given by Castagné [19]. The flow stress can be written as [13]

$$\tau_1 = \frac{\gamma}{b}\left(\frac{2\bar{R}_z}{L_F}\right). \tag{15}$$

Dealing with superlattice dislocations, Brown and Ham [13] have shown that when the first dislocation of a superlattice dislocation pair meets the Friedel condition, the second dislocation is pulled forward by the anti phase boundary remaining in the particles which it intersects by τ_{APB} described by

$$\tau_{APB} = f\frac{\gamma}{b}. \tag{16}$$

The applied flow stress required for cutting the precipitates, τ_a, follows from

$$2\tau_a - \tau_1 + \tau_{APB} = 0. \tag{17}$$

Taking the experimental values mentioned before (f, $\bar{R}$, γ) and $L_{NMR} \simeq L_F = 0.08\,\mu$m, τ_a is found to be 29 MPa. This is in close agreement with the increase of the applied yield stress ($\tau_a \simeq \sigma_a/3$) of Al–Li (aged at 215°C, 1 h) compared to ultrapure Al. As a matter of course, this increase should be compared with the as-quenched sample value. However, we could not obtain very reproducible results for those samples as far as the yield stress is concerned (12–28 MPa). Orowan looping will occur when $\tau_a = \frac{1}{2}\tau_0$. τ_0 [20, 21] is calculated to be 97 MPa. It means that as long as $\gamma_{APB} \leqslant 180\,\text{mJ/m}^2$ shearing of the precipitates will take place.

In calculating the critical stress for looping in Al–Li aged at 245°C (115 h) the average gap between the precipitates is assumed to be $L_{NMR} \simeq 0.25\,\mu$m. τ_0 is calculated to be 31.4 MPa. Since the applied stress required for cutting [equation (17)] is much larger than $\tau_0/2$ the first dislocation within the superlattice dislocation pair reaches the looping stage. The connection between L_{NMR} and L_p, the average gap between the precipitates, will be discussed in Section 4.3.

4.2. Activation length

Mechanical tests involving a change in strain rate by a factor of ten were employed to measure $(\delta \ln\dot{\epsilon}/\delta\tau)_T$ [equation (5)], from which the apparent activation volume was deduced. The resulting data, depicted in Fig. 9, reveal that the apparent activation

volume and activation length for each alloy system decreases with increasing strain. This behaviour has been observed also in f.c.c. crystals using the same techniques, e.g. in Al by Mukherjee *et al.*, [22] and in Cu by Van Den Beukel and co-workers [23]. However, there exists a striking difference between the two Al–Li alloy systems with respect to the rate at which this decrease happens. This can be understood by the following arguments: the effective activation length represents the mean spacing of the forest dislocations [24]. As mentioned before in 4.1 in the Al–Li alloy containing shearable precipitates work-softening will take place [14], i.e. the slip will tend to be heterogeneous in such a material.

The tendency to produce heterogeneous slip will be more pronounced the more the flow stress resistance decrease by the passage of a dislocation. Once the δ' precipitates are sheared their resistance to further dislocation motion is reduced and strain localization will occur. It is obvious that under heterogeneous slip less rapid formation of stable dislocation configurations can arise as a result of reactions between the sets of slipping dislocations. The rate of strain hardening, based on the concept that the slipping dislocations interact to produce low energy configurations which then restrain motion of slipping dislocations, is expected to be small in the case of shearable δ' precipitates. This is in agreement with the experimental observations (Fig. 8). These findings are in contrast to the strain dependence of λ measured in Al–Li where Orowan loops are formed. In this material dislocation bypassing occurs and the workhardening of this slip plane leads to slip homogenization. On straining dislocation debris accumulates round the particles leading to workhardening of the slip plane upon which the dislocations have moved. It favours therefore the operation of a different slip plane, i.e. slip tends to become homogeneous. The workhardening is due to Orowan loops at low strains and to an increasing degree, due to prismatic loops at high strains [25, 26]. With increasing strain the number of prismatic loops increases, and therefore the length of the obstacles in slip plane increase, leading to a self-hardening of the slip line. At large strains even loops can be punched out on secondary systems (due to the back stress from the prismatic loops) and plastic zones of considerable complexity are formed leading to *forest hardening* [27]. Because these various hardening mechanisms are operative in Al–Li containing nonshearable precipitates, the activation length is expected to decrease with strainhardening more rapidly than in Al–Li containing shearable precipitates. Indeed, this is confirmed by the experimental observations depicted in Fig. 9. It should be noted that in the derivation of the activation length λ it was assumed that the obstacle width was independent of the applied stress and has the arbitrarily chosen value of b. In the Friedel approximation the effective activation length is proportional to the applied stress $\tau^{-1/3}$ [28]. This effective spacing is given approximately by

$$\lambda_F = \left(\frac{2T}{\tau b L_s}\right)^{1/3} L_s \tag{18}$$

where L_s is the mean square spacing [equation (8)]. (For shearable precipitates λ_F is actually identical to L_F. Substituting the mean square spacing [equation (8)] and $\tau = \tau_i$ [equation (15)] into equation (18) one arrives at equation (9)]. Based on equation (18) the activation volume will become equal to $2/3\ \lambda b^2$ leading to somewhat higher values of λ than depicted in Fig. 9.

4.3. Comparison between mean jump distance and activation length

In conclusion we may say that there exists mutual consistency between the main jump distance and the activation length as far as their effects on the hardening rates are concerned. However, there are considerable differences in magnitude between the activation length λ and the mean jump distance L in the two alloy systems. For instance, in the alloy (b) containing nonshearable precipitates $L_{NMR} > \lambda$ for $\epsilon > 5\%$ whereas in the alloy (a) containing shearable precipitates $L_{NMR} < \lambda$ over the whole range of deformation. In principle there is no physical reason why the mean activation length λ and mean jump distance L_{NMR} in these alloy systems should be identical. Precipitates, both shearable and nonshearable, cannot be passed by due to thermal fluctuations as in a strain rate-change experiment. Therefore, λ is determined by the forest dislocation density and Li impurities in solid solution. On the other hand, L_{NMR} depends on both the average gap between the precipitates and mean spacing between the forest dislocations. L is obtained from samples which are deformed with *constant*

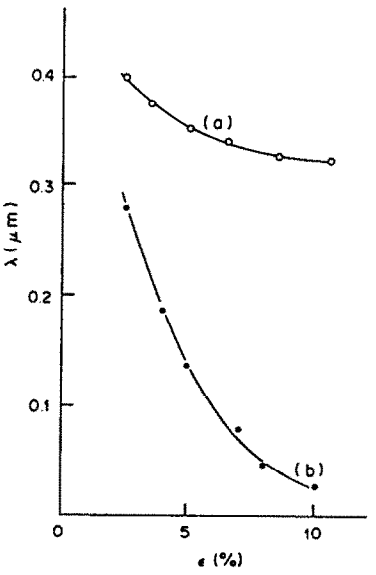

Fig. 9. Activated length determined from strain rate change experiments. The strain rate range is 10^{-6} to $10^{-1}\ s^{-1}$. (a) Al–Li (2.2 wt%) aged at 215°C (1 h), (b) Al–Li (2.2 wt%) aged at 245°C (115 h).

strain rate $\dot{\epsilon}$ with increasing stress. This means that L is dynamically influenced by dislocation multiplication. The mean distance covered during a dislocation jump is controlled merely by relatively hard obstacles (precipitates, forest dislocations) since the effective stress is large enough to make the soft obstacles (Li in solid solution) contribute to the lattice friction only. *Changes in strain rate* during deformation, however, can cause similar effects to the flow stress as changes in temperatures. An increase in strain rate gives less time for thermally activated events: i.e. it is equivalent to a lowering of the temperature of deformation. As a consequence, hardening occurs because dislocations blocked by forest dislocations in the primary slip plane are not able to avoid them by cross slip. In addition, the cooperative way of dislocation dynamics will influence λ. A dislocation pinned at different obstacles may "unzip" along its entire length after thermal activation of only one segment of the dislocation across one barrier, since at that very moment the critical breakaway angle of all other segments is exceeded. Only a small activation volume V per segment would be measured and consequently a small λ, although L_{NMR} in that case need not be influenced by this unzipping effect.

A plausible connection between λ and L_{NMR} can be based on the following model: all moving dislocations, delayed at intersections with either forest dislocations or precipitates, affect the spin-lattice relaxation rate. Assuming two different sets of corresponding mobile dislocation densities: ρ_1 and ρ_2, respectively, the total spin lattice relaxation rate can be written as

$$\left(\frac{1}{T_{1\rho}}\right)_D = \left(\frac{1}{T_{1\rho}}\right)_D^{(1)} + \left(\frac{1}{T_{1\rho}}\right)_D^{(2)} \tag{19}$$

where [see equation (3)]

$$\left(\frac{1}{T_{1\rho}}\right)_D^{(1)} \approx \frac{\rho_1}{L_1\rho} \quad \text{and} \quad \left(\frac{1}{T_{1\rho}}\right)_D^{(2)} \approx \frac{\rho_2}{L_2\rho} \tag{20}$$

and $\rho_1 + \rho_2 = \rho$. L_1 represents the spacing between forest dislocations, λ, and L_2 is the gap between the precipitates, L_p. In equation (19) the contribution to the spin-lattice relaxation rate due to any movement of dislocation debris accumulated round the precipitates has been neglected. At $\epsilon = 5\%$ alloy (b), λ is found to be $0.14\,\mu$m and the average gap between the nonshearable precipitates $L_p = 0.3\,\mu$m. Assuming equal fractions ($\rho_1 = \rho_2$). the mean jump distance L_{NMR} is calculated to be $0.19\,\mu$m, according to

$$\frac{1}{L_{NMR}} \simeq \frac{\rho_1}{\lambda\rho} + \frac{\rho_2}{L_p\rho}. \tag{21}$$

This is almost equal to the experimentally determined value (Fig. 2). From equation (21) follows that, providing $\rho_1 \neq 0$, L_{NMR} is always smaller than the gap between the precipitates L_p (= constant). Assuming equal fractions ($\rho_1 = \rho_2$) up to $\epsilon = 10\%$, L_{NMR} is predicted to be $0.07\,\mu$m ($\lambda = 0.04\,\mu$m, $L_p = 0.3\mu$m). Again, this is in agreement with experiments (Fig. 2). Based on the experimental values of λ and L_p, L_{NMR} should be larger than λ in the alloy containing nonshearable precipitates.

An Al–Li containing shearable precipitates (alloy a) the relationship between L_{NMR} and λ is more complicated. In this case L_{NMR} and λ are almost constant over the whole range of deformation. On the contrary, L_p depends on ϵ since the cross section of the precipitate in the slip-plane will be reduced upon deformation. Further, it is likely that moving dislocations inside the precipitates contribute to the spin-lattice relaxation rate separately. When a mobile dislocation crosses over a distance L_p and subsequently short jumps occur over a distance $\bar{d}$, the mean diameter of the precipitates, the total spin lattice relaxation rate measured by NMR is largely determined by the jump distance inside the precipitates: ($\bar{d} < L_p \ll \lambda$)

$$\frac{1}{L_{NMR}} \simeq \frac{\rho_1}{\lambda\rho} + \frac{\rho_2}{L_p\rho} + \frac{\rho_3}{\bar{d}\rho} \tag{22}$$

apparently leading to $L_{NMR} < \lambda$.

5. CONCLUSIONS

It turned out that pulsed nuclear magnetic resonance is a complementary new technique for the study of moving dislocations in Al–Li alloys. Spin-lattice relaxation measurements clearly indicated that the fluctuations in the quadrupolar field due to moving dislocations in alloys containing either shearable or nonshearable precipitates are quite different. The NMR experiments provided information of the mean jump distance of dislocations in these alloys. Transmission electronmicroscopic observations of the mean planar diameter of the precipitates, in combination with the NMR data, predicted the increase of the yield stress compared to ultrapure aluminium in reasonable agreement with experiment. It was found that the activation length, obtained from mechanical strain rate change experiments, have different values compared to the measured values of the mean jump distance determined by NMR. Reasons for the mean jump distance being different from activation length have been given. Nevertheless, both mean jump distance and activation length have been found to decrease with strain hardening more rapidly in Al–Li containing nonshearable precipitates than in Al–Li containing shearable precipitates. These findings are consistent with the experimentally measured workhardening rates.

Finally, it should be emphasized that Al–Li alloy is not an alloy system that exhibits only one type of hardening: i.e. order hardening or Orowan hardening. Plastic deformation is a local process and as a consequence depends on the local characteristics of the microstructure. Since there exists a distribution of particle sizes both hardening mechanisms may occur. Nonetheless, NMR measurements clearly showed different fluctuations in the local magnetic field due

to moving dislocations in these two alloys from which a difference in dislocation dynamics may be concluded.

Acknowledgements—The authors should like to thank Professor A. Van Den Beukel for valuable discussion and for critical reading of the manuscript. Thanks are due to Dr L. Katgerman (Technological University, Delft), providing us with the raw Al–Li material. We thank Mr U. Schlagowski for the technical assistance in the NMR measurements. The work is part of the research program of the Foundation for Fundamental Research on Matter (F. O. M., Utrecht) and has been made possible by financial support from the Netherlands Organization for the Advancement of Pure Research (Z. W. O., The Hague) and the Deutsche Forschungsgemeinschat, F.R.G.

REFERENCES

1. *Proc. Conf. Aluminium–Lithium Alloys* (edited by T. N. Sanders and E. A. Starke), Am. Inst. Min. Engrs, New York (1981).
2. T. H. Sanders and E. A. Starke, *Acta metall.* **30**, 927 (1982).
3. J. Th. M. De Hosson, O. Kanert, A. W. Sleeswyk, in *Dislocations in Solids* (edited by F. R. N. Nabarro), Vol. 6, Chap. 32, pp. 441–534. North-Holland, Amsterdam (1983).
4. H. Tamler, O. Kanert, W. H. M. Alsem and J. Th. M. De Hosson, *Acta metall.* **30**, 1523 (1982).
5. H. J. Hackelöer, O. Kanert, H. Tamler and J. Th. M. De Hosson, *Rev. scient. Instrum.* **54**, 341 (1983).
6. J. Th. M. De Hosson, W. H. M. Alsem, H. Tamler and O. Kanert, in *Defects, Fracture and Fatigue* (edited by G. C. Sih and J. W. Provan), p. 23. Nijhoff, The Netherlands (1982).
7. E. Orowan, *Z. Phys.* **89**, 634 (1934).
8. U. F. Kocks, A. S. Argon and M. F. Ashby, in *Progress in Materials Science* (edited by B. Chalmers, J. W. Christian and T. B. Massalski), Vol. 19, p. 1. Pergamon Press, Oxford (1975).
9. J. Th. M. De Hosson, O. Kanert and H. Tamler, in *Aluminium–Lithium Alloys* (edited by T. H. Sanders and E. A. Starke). Am. Inst. Min. Engrs, New York (1983).
10. O. Kanert and M. Mehring, *Static Quadrupole Effects in Disordered Cubic Solids, NMR*, Vol. 3. Springer, Berlin (1971).
11. U. F. Kocks, in *Fundamental Aspects of Dislocation Theory* (edited by J. A. Simmons, R. De Wit and R. Bullough), Vol. 2, p. 1077. NBS Spec. Publ. 317. (1970).
12. D. J. H. Cockayne, *Z. Naturf.* **27a**, 452 (1972).
13. L. M. Brown and R. K. Ham, in *Strengthening Methods in Crystals* (edited by A. Kelly and R. B. Nicholson), p. 12. Appl. Sci. Publ., London (1971).
14. J. W. Martin, *Micromechanisms in Particle-Hardened Alloy*. Cambr. Solid St. Sci. Ser., Cambridge (1980).
15. M. Tamura, T. Mori and T. Nakamura, *Trans. Japan Inst. Metals* **14**, 355 (1973).
16. M. F. Ashby, *Phil. Mag.* **21**, 399 (1970).
17. K. C. Russell and M. F. Ashby, *Acta metall.* **18**, 891 (1970).
18. A. W. Thompson, M. I. Baskes and W. F. Flanagan, *Acta metall.* **25**, 1017 (1973).
19. J. L. Castagné, *J. Physique* **27**, C3-233 (1966).
20. P. B. Hirsch and F. J. Humphreys, *The Physics of Strength and Plasticity* (edited by A. S. Argon). M.I.T. Press, MA (1969).
21. P. M. Kelly, *Int. Metall. Rev.* **18**, 31 (1973).
22. A. K. Mukherjee, J. D. Mote and J. E. Dorn, *Trans. metall. Soc. A.I.M.E.* **233**, 1559 (1965).
23. G. Den Otter, Thesis, Technological University Delft, (1978); G. Den Otter and A. Van Den Beukel, *Physica status solidi* (a) **55**, 785 (1979).
24. A Seeger, *Dislocation and Mechanical Properties of Crystals*, pp. 243–332. Wiley, New York (1956).
25. P. B. Hirsch, in *The Physics of Metals*, Vol. 2, p. 189. Cambridge Univ. Press (1975).
26. P. B. Hirsch and F. J. Humphreys, *Proc. R. Soc.* **A318**, 45 (1970).
27. M. F. Ashby, *Strengthening Methods in Crystals* (edited by A. Kelly and R. B. Nicholson), p. 137. APPL. Sci., London (1971).
28. J. Friedel, *Dislocations*. Pergamon Press, New York (1964).